J Mol Model (2009) 15:1463–1479
DOI 10.1007/s00894-009-0498-x

ORIGINAL PAPER

Use of molecular modeling, docking, and 3D-QSAR studies for the determination of the binding mode of benzofuran-3-yl-(indol-3-yl)maleimides as GSK-3β inhibitors

Ki Hwan Kim · Irina Gaisina · Franck Gallier · Denise Holzle · Sylvie Y. Blond · Andrew Mesecar · Alan P. Kozikowski

Received: 30 October 2008 / Accepted: 16 April 2009 / Published online: 14 May 2009

Abstract Molecular modeling and docking studies along with three-dimensional quantitative structure relationships (3D-QSAR) studies have been used to determine the correct binding mode of glycogen synthase kinase 3β (GSK-3β) inhibitors. The approaches of comparative molecular field analysis (CoMFA) and comparative molecular similarity index analysis (CoMSIA) are used for the 3D-QSAR of 51 substituted benzofuran-3-yl-(indol-3-yl)maleimides as GSK-3β inhibitors. Two binding modes of the inhibitors to the binding site of GSK-3β are investigated. The binding mode 1 yielded better 3D-QSAR correlations using both CoMFA and CoMSIA methodologies. The three-component CoMFA model from the steric and electrostatic fields for the experimentally determined pIC_{50} values has the following statistics: R^2(cv)=0.386 nd SE(cv)=0.854 for the cross-validation, and R^2=0.811 and SE=0.474 for the fitted correlation. F (3,47)=67.034, and probability of R^2=0 (3,47)=0.000. The binding mode suggested by the results of this study is consistent with the preliminary results of X-ray crystal structures of inhibitor-bound GSK-3β. The 3D-QSAR models were used for the estimation of the inhibitory potency of two additional compounds.

Keywords Benzofuran-3-yl-(indol-3-yl)maleimides · Binding mode · CoMFA · CoMSIA · Docking · GSK-3beta inhibitors · 3D-QSAR · X-ray

K. H. Kim (✉) · I. Gaisina · F. Gallier · A. P. Kozikowski
Drug Discovery Program, Department of Medicinal Chemistry and Pharmacognosy, College of Pharmacy,
University of Illinois at Chicago,
833 S. Wood St.,
Chicago, IL 60612, USA
e-mail: pkhkim@gmail.com

D. Holzle · S. Y. Blond · A. Mesecar
The Center for Pharmaceutical Biotechnology,
Department of Medicinal Chemistry and Pharmacognosy, College of Pharmacy,
University of Illinois at Chicago,
900 South Ashland,
Chicago, IL 60607, USA

Introduction

Originally identified as a modulator of glycogen metabolism about 20 years ago, glycogen synthase kinase 3β (GSK-3β) is now found to be a Ser/Thr protein kinase with key roles in transduction of regulatory role in a variety of pathways. These include the initiation of protein synthesis, cell proliferation, cell differentiation, and apoptosis. This kinase is also essential for embryonic development [1–4]. In humans, two genes are present that encode the related GSK-3 isoforms GSK-3α and GSK-3β, which exhibit approximately 98% sequence identity within their catalytic domains.

Many different kinds of GSK-3 inhibitors have been studied by various researchers [4–27]. Our attention was directed to the discovery of inhibitors of the GSK-3β to be used possibly in the treatment of a number of CNS disorders including Alzheimer′s disease, Parkinson′s disease, bipolar disorders, and traumatic brain injury. Our work in this area was influenced by the maleimide-bearing natural product staurosporine [19, 24].

In our previous paper, we reported on the chemical synthesis and the biological activities of a number of substituted maleimides as inhibitors of GSK-3β and additionally examined their selectivity for inhibition of CDK2/cyclinE [28]. In this paper, we report on our study of the molecular modeling and docking of the inhibitors into the binding site of GSK-3β, together with 3D-quantitative structure-activity relationships (3D-QSAR) using the comparative molecular field analysis (CoMFA) [29–31] and the comparative molecular similarity indices analysis (CoMSIA) [32]. A specific aim of this study is to identify the correct binding mode of the substituted maleimide compounds included in this study using the computer-aided molecular modeling techniques. Fifty-one 3-benzofuranyl-4-indolyl-maleimide-based GSK-3β inhibitors of structural type I are included in the present work. Two possible binding modes are examined to determine the correct interaction mode of these compounds with the enzyme. Superpositions of the two alignments are obtained by docking the inhibitors to the known X-ray crystal structure of GSK-3β (1R0E), where a similar ligand to our inhibitors is bound.

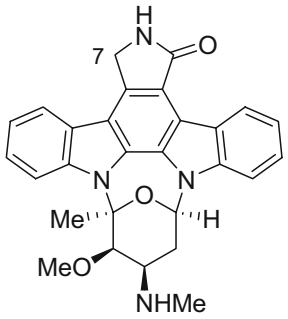

Staurosporine

Results and discussion

Studies on the binding mode of the inhibitors

In order to study the binding mode of the inhibitors, we chose to utilize 3D-QSAR methodologies. For such 3D-QSAR studies employing both the CoMFA or CoMSIA methodologies, all compounds need to be superimposed under the assumption that they bind in a similar manner to the same binding site. Different methods have been used in the literature for the superposition of the compounds of interest. We decided to dock the inhibitors to the binding site of GSK-3β protein and use the docked conformation of the inhibitors in our CoMFA and CoMSIA studies. In previous publications from this laboratory we assumed that the binding mode of the substituted maleimides, either indol-3-yl-(indazol-3-yl)maleimides or benzofuran-3-yl-(indol-3-yl)maleimides, is similar to that found for staurosporine in its X-ray co-crystal structure with GSK-3β (1Q3D) [33].

In this study, we reinvestigated the possible binding mode of the benzofuran-3-yl-(indol-3-yl)maleimides (I) to GSK-3β in an effort to develop a potent and selective GSK-3β inhibitor. In order to find relevant information about the binding mode and conformation of the inhibitors, we first examined the known X-ray crystal structures of GSK-3β currently available in the RCSB PDB Protein Data Bank [34]. Table 1 lists the X-ray structures of the GSK-3β complexes that were examined. Four of the eight ligands in Table 1 are similar to our GSK-3β inhibitors.

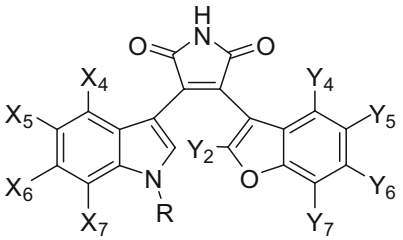

(I)

Examination of the X-ray crystal structures of GSK-3β in Table 1 revealed that there are roughly two types of GSK-3β structures with respect to Phe67: one is 1R0E-like (in yellow), and the other is 1Q4L-like (in orange) (Fig. 1a). Between these two extreme structures, there are intermediate ones like that represented by the 1Q41 structure (Fig. 1b, in pink). The changes in position of the Phe67 residue are due to the differences in the conformation of the Gly-rich loop observed in essentially all Ser/Thr and Tyr protein kinase structures [35–37]. Another major change in the conformations observed among these structures is the movement of the Arg141 side chain (see the discussion below). The side chain movements of Arg141 in the GSK-3β structures can be seen at the lower left corner of Fig. 1b.

Table 1 Known GSK-3β X-ray structures

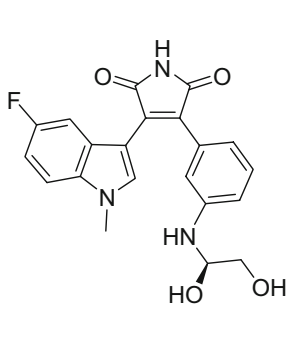

(II)

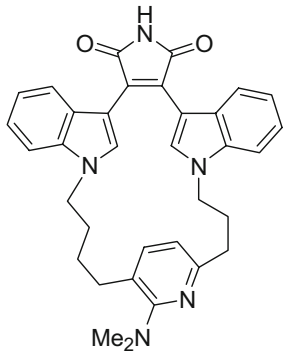

(III)

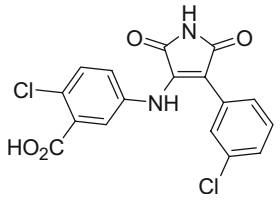

(IV)

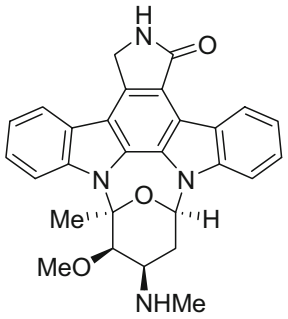

(V)

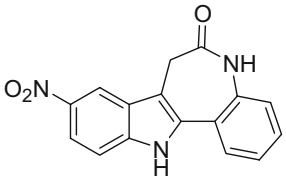

(VI)

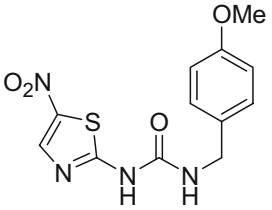

(VII)

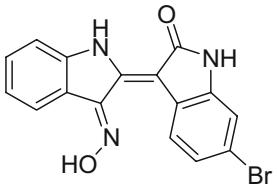

(VIII)

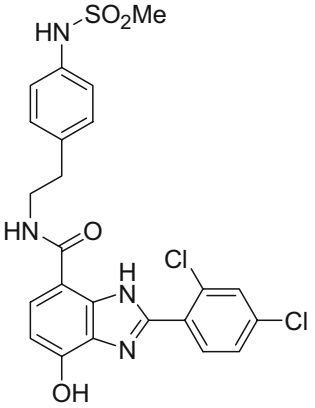

(IX)

	Group	PDB	Resolution	R-value	Bound Ligand	Ref
A.	1R0E-like	1R0E	2.25	0.225	(II)	[47]
		2OW3	2.80	0.248	(III)	[48]
		1GNG	2.60	0.196		[49]
		1O9U	2.40	0.233		[50]
B.	1Q4L-like	1Q4L	2.77	0.212	(IV)	[51]
		1H8F	2.80	0.220		[52]
		1I09	2.70	0.242		[53]
		1J1B	1.80	0.216		[54]
		1J1C	2.10	0.218		[54]
		1Q3D	2.20	0.230	(V: Staurosporine)	[51]
		1Q3W	2.30	0.225	(VI)	[51]
		1Q5K	1.94	0.222	(VII)	[55]
		1UV5	2.80	0.193	(VIII)	[6]
		1PYX	2.40	0.206		[51]
		1Q41	2.10	0.229		[51]
		2O5K	3.20	0.240	(IX)	[23]

The binding mode of staurosporine, the compound that the design of our inhibitors was initially influenced by, is shown in Fig. 1c. The X-ray crystal structure shows that the binding pose of the staurosporine is guided by the two adjacent intermolecular hydrogen bonds of the pyrrolidin-2-one moiety. The NH group of the pyrrolidin-2-one ring of staurosporine forms a hydrogen bond to the backbone carbonyl oxygen of Asp133, and the carbonyl oxygen of

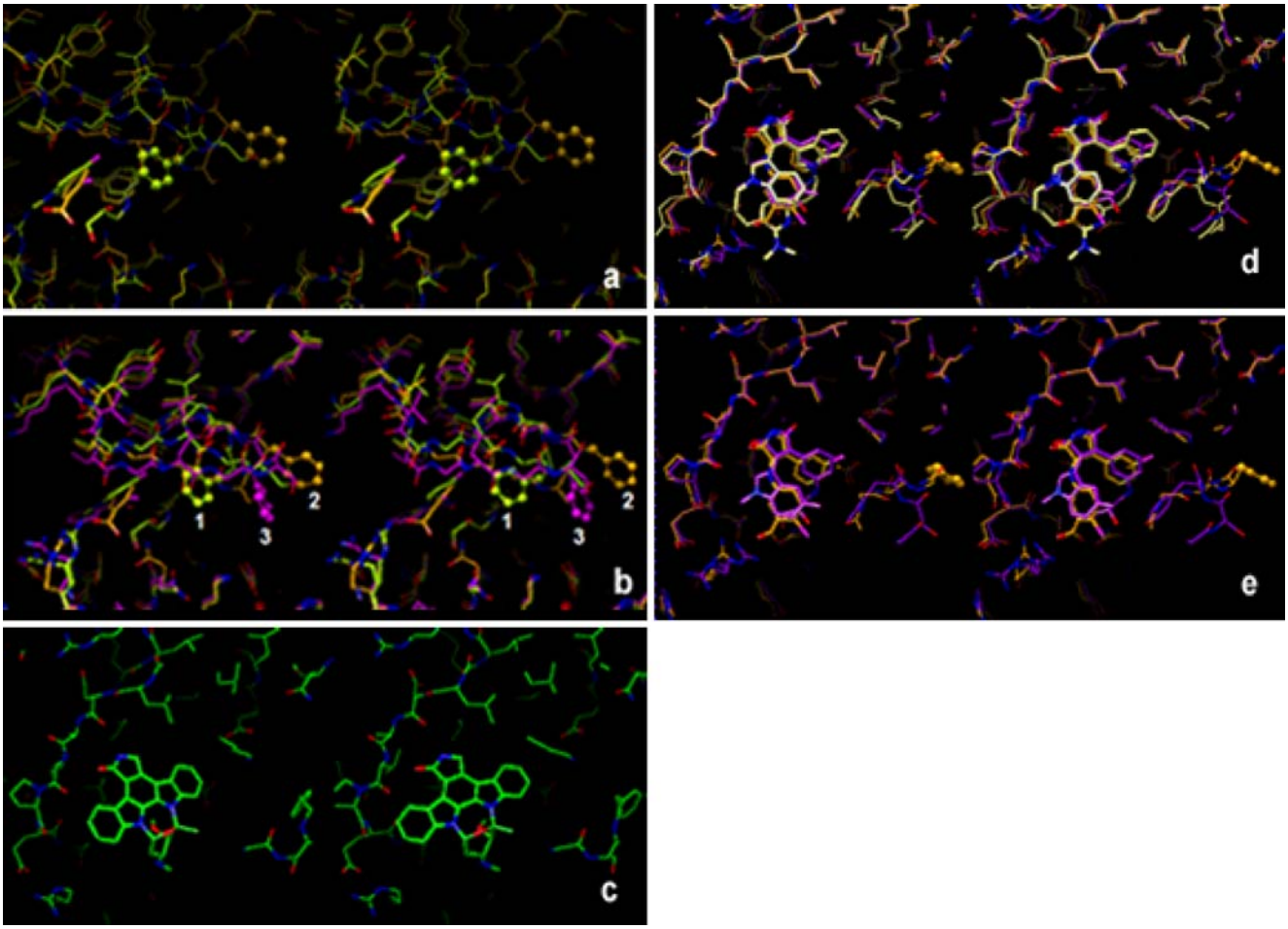

Fig. 1 X-ray crystal structures of ligand-bound GSK-3β structures listed in Table 1. (**a**) Approximately two groups of GSK-3β structures are shown with respect to the residue Phe67: one is 1R0E-like (yellow), and the other is 1Q4L-like (orange). The two groups of Phe67 positions of GSK-3β structures are illustrated by the two different positions of the phenyl ring shown in the ball-and-stick model in Fig. 1a (labeled **1** and **2** in Fig. 1b). (**b**) Between the two extreme structures shown in (**a**), there are intermediate ones represented by 1Q41 in pink (labeled **3** in Fig. 1b). The phenyl ring of this intermediate ones of GSK-3b is illustrated by the phenyl ring (ball-and-stick model in pink) shown between the two different positions of the phenyl rings shown in Fig. 1a. Multiple conformations of Arg141 can be seen at the lower left corner. (**c**) Binding mode of staurosporine (1Q3D). (**d**) Binding modes of II (1R0E), III (2OW3), and IV (1Q4L) from the superimposed GSK-3β structures. They show similar binding conformation of the three compounds. (**e**) Binding modes of II and IV showing similar binding conformation of these two compounds

the same ring forms a hydrogen bond to the backbone NH of Val135. Hydrophobic side chains of Leu132 and Lys85 are present around the methylene group (carbon 7 indicated in the staurosporine structure) of staurosporine. In addition, there are two water molecules connecting the carbonyl oxygen of the pyrrolidin-2-one moiety and Glu97 nearby. The two indole rings of staurosporine are fixed by a phenyl group connecting the two rings, and so do their binding positions.

Figure 1d shows the binding modes of II, III, and IV in Table 1. Compound III has two indole rings as does staurosporine, whereas II has only one indole ring, and IV has an aminophenyl and a phenyl ring instead of the two indole rings. The two indole rings in III are partially rigidified through macrocycle formation encompassing the two indole rings. Even though the two indole rings are semi-rigid, the binding conformations of the two indole rings of III are significantly different from that of staurosporine, and similar to those of II and IV.

Figure 1e shows the binding modes of II and IV. The indole ring conformation of II is very similar to that of III as well as that of the aminophenyl ring of IV. The conformation of the phenyl ring of II and IV is similar to one another.

Based on the X-ray structures of II, III, and IV, we proposed that the binding mode of benzofuran-3-yl-(indol-3-yl)maleimides (I) in Table 6 would be similar to those of II, III, and IV. This is contrary to the binding mode suggested in the earlier publications for 3-indolyl-4-indazolylmaleimides or benzofuran-3-yl-(indol-3-yl)

maleimides [19, 24]. Since the indole ring of II is on the left side and the substituted phenyl ring of II or IV is on the right side in Fig. 1d, it was thought that the indole ring of the maleimides in Table 6 is on the left and the benzofuran ring is on the right in this view. Therefore, all 51 maleimides in Table 6 were docked into the binding site of GSK-3β (1R0E) in this postulated manner. We chose the GSK-3β structure of 1R0E for our docking study, because its bound ligand is the most similar to our inhibitors. The binding conformation of the benzofuran ring could be similar to that of the indole ring of III if the substituent on the benzofuran ring is not large. However, if the substituent on the benzofuran ring is of sufficient bulk, then there is not enough space for the conformation observed for III. In such a case, the benzofuran ring would be rotated by 180º. For the purpose of the CoMFA and CoMSIA studies, the conformation of the rotated benzofuran ring was selected, because some of our inhibitors have a larger substituent than can be accommodated by the pocket present in the unrotated-binding conformation. When a large substituent is present at the X5 position of the indole ring of the benzofuran-3-yl-(indol-3-yl)maleimide, the substituent would clash sterically with Phe67, which would result in the movement of the glycine-rich loop. The consequence of this movement would result in the conformational change of Phe67 from the position of 1R0E-like structure to the position of 1Q4L-like structure (see Fig. 1a). For consistency, all the compounds listed in Table 6 were docked in this conformation to the GSK-3β binding site. (See further discussion below.) The starting conformation of the initial conformation of each compound was manually superimposed over the pyrrolidin-2-one ring of the ligand-bound GSK-3β structure (1R0E) because of the reason discussed above.

Even though the binding mode of the compounds in Table 6 is likely to be the one (binding mode 1) described above, we decided to investigate other possible binding modes, especially in light of the fact that a different binding conformation was previously proposed [19, 24, 56]. First, we examined the relative conformational energy of different possible binding conformations of an unsubstituted benzofuran-3-yl-(indol-3-yl)maleimide to the GSK-3β binding pocket. Figure 2 shows eight different binding modes with four different conformations that are possible in the GSK-3β binding site. In 2a and 2b in Fig. 2, the positions of the indole and the benzofuran rings are switched. With respect to the indole and the benzofuran ring positions, the conformations 2a and 2b in Fig. 2 are the same when only the ligand is considered, but they would be different in the binding site. The conformational energies of these conformations are summarized in Table 2.

The conformational energy differences among these four conformers are very small, thus suggesting that any of these conformers may represent their actual binding conformation to the GSK-3β. Nonetheless, it is interesting to note that conformation 2a (and 2b), which is the one believed to represent the likely binding mode of the compounds in Table 6, has the lowest conformational energy. Among the eight possible binding modes shown in Fig. 2, binding modes 2a and 2b are the two most likely binding modes based upon an analysis of the known ligand-bound GSK-3β X-ray crystal structures as discussed above. Therefore, we chose to investigate 3D-QSAR based on these two binding modes in order to determine the binding mode of these compounds.

Comparative molecular field analysis

The 51 compounds included in this study are listed in Table 6 along with the IC_{50} values toward GSK-3β. The IC_{50} values were determined for their potency to inhibit GSK-3β. Commercially available human GSK-3β, was assayed for its ability to phosphorylate the primed peptide substrate (RRRPASVPPSPSLSRHSS(P)HQRR; 10 μM) in the presence of 0–10 μM of the maleimides [57]. The inhibitory potency expressed as pIC_{50} values is the negative logarithm of IC_{50} value. Therefore, the larger the pIC_{50} value is, the more potent the compound is as an inhibitor of the kinase. The two binding modes (2a and 2b in Fig. 2) of these compounds were obtained by docking each molecule into the binding site of GSK-3β starting from two different initial binding conformations as described above.

I. CoMFA for binding model 1

Figure 3 shows all the compounds superimposed of the docked conformation in binding mode 1. Binding mode 1 corresponds to the conformation 2a shown in Fig. 2. The best CoMFA model of the 51 substituted maleimides obtained is a three-component model from the steric and electrostatic fields with the following statistics (see Table 3): R^2(cv)=0.386 and SE(cv)=0.854 for the cross-validation, and R^2=0.811 and SE=0.475 for the fitted. F (3,47)= 67.034, and Prob. of R^2=0 (3,47)=0.000. The steric component of these maleimide analogs on the inhibitory potency described by this model is 48%, whereas the electrostatic portion is 52%. The first component explains 51% of the variance in the pIC_{50}, and the second and the third components account for additional 22% and 8% of the variance, respectively. An essentially identical CoMFA model was obtained when the steric and the electrostatic fields were considered separately.

In our previous unpublished study, the classical QSAR result shown below was obtained [28]. It is interesting that the statistical quality (R^2 and SE) of the classical QSAR

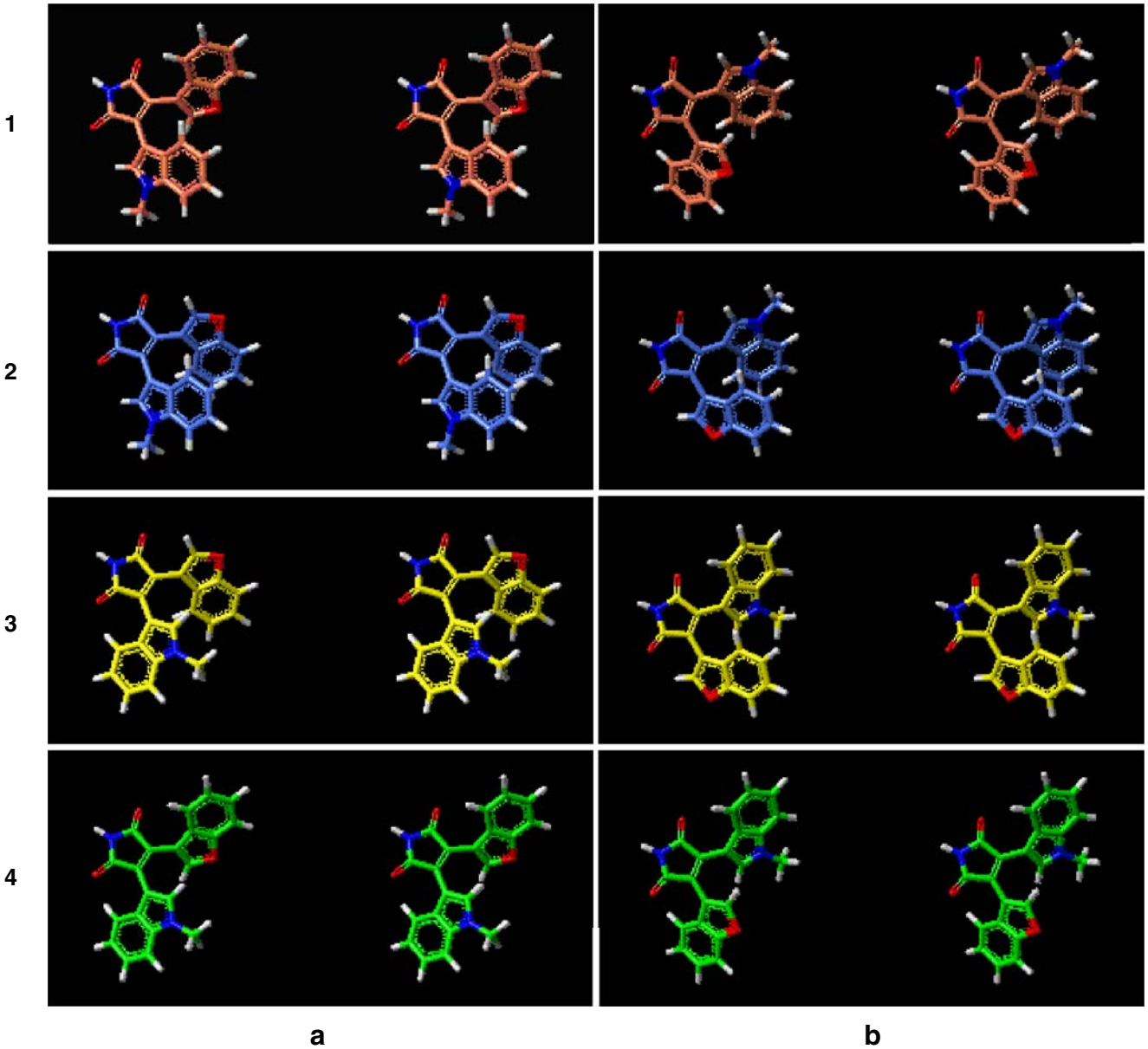

Fig. 2 Four representative conformations (**1**–**4**) of benzofuran-3-yl-(indol-3-yl)maleimides in binding mode 1 (**a**) and 2 (**b**)

and the 3D-QSAR method using the CoMFA methodology is similar. One compound (compound 1 in Table 6) was treated as an outlier in the classical QSAR, but this compound was included in the CoMFA study.

Table 2 Relative conformational energy of four representative conformations of 3-(benzofuran-3-yl)-4-(indol-3-yl)maleimides shown in Fig. 2

Binding mode 1	Binding mode 2	ΔEnergy (kcalmol^{-1})
1a	1b	1.6
2a	2b	0.0
3a	3b	1.4
4a	4b	2.1

$$pIC_{50} = -0.60\ (\pm 0.18)\ \pi_{Y6} + 0.51\ (\pm 0.12)\ (\pi_{Y6})^2 + 1.78(\pm 0.21)\pi_{X5} - 0.07(\pm 0.01)(C\log P)^2 + 0.10(\pm 0.02)\ MR_r - 0.86(\pm 0.17)(\pi_{X5})^2 - 1.18(\pm 0.38)\sigma p_{X6} + 0.49\ (\pm 0.24)\pi_R + 0.34(\pm 0.24)\pi_{X7} + 7.60(\pm 0.30),\ N = 50,\ R^2 = 0.842,\ RMSE = 0.436$$

Figure 4 is the coefficient contour map of the three-component model derived from all 51 compounds. In this contour map, the sterically favored regions are shown in green, and the sterically disfavored regions are shown in yellow. The positive electrostatic contours are shown in blue, and the negative electrostatic contours are shown in red. Table 6 shows the observed and the calculated pIC_{50} values from this three-component CoMFA model along with their observed values. It is interesting to note that

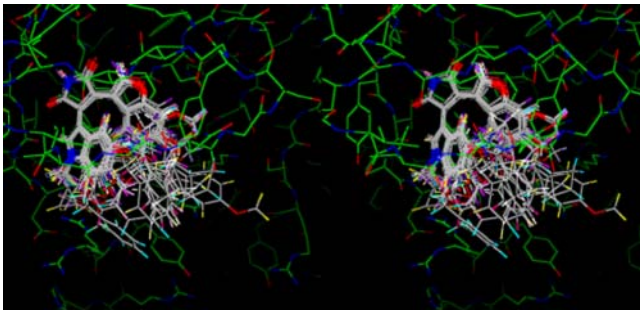

Fig. 3 Superposition of 51 substituted maleimides as GSK-3β inhibitors obtained from docking into the binding site of GSK-3β structure (1R0E) in binding mode 1

there is a sterically favored region in the steric contour map (colored in green in Fig. 4a) near the Y2 position of the benzofuran-3-yl-(indol-3-yl)maleimide. The hydrophobic residue Leu132 and the four methylene groups of Lys85 are located near the X2 group and the adjacent carbonyl group of the pyrrolidine-2-one ring. This indicates that a hydrophobic group at this position may improve the inhibitory potency of the compound. As is the case for the binding orientation of staurosporine observed in Fig. 1c (1Q3D), the binding orientation of the GSK-3β inhibitors in Table 6 is fixed by the two hydrogen bonds involving the pyrrolidin-2-one rings of the inhibitors. One of the carbonyl oxygens (left one in Fig. 3) of the pyrrolidin-2-one ring forms a hydrogen bond with the backbone NH of Val135, and the NH group of the pyrrolidin-2-one ring interacts with the backbone carbonyl group of Asp133 residue. Both residues are in the hinge region of GSK-3β.

Four compounds (**1**–**4**) in Table 6 have IC_{50} values in sub-nanomolar inhibitory potency. Compounds **2**, **3**, and **4** have a 6-CH_2OH at the Y6 position, and compound **1** has a 7-CH_2OMe at the X7 position. There are other compounds with 6-CH_2OH at the Y6 position among the compounds in Table 6. These compounds are in general potent inhibitors. Two compounds (**7** and **8**) have a similar substituent 7-CH_2OH at X7 position to the 7-CH_2OMe of Compound **1**.

Figure 5 shows the binding site amino acid residues around the 7-CH_2OH group at X7 position and the 6-CH_2OH at Y6 position of Compound **2** or **8** as a representative case, respectively. The 7-CH_2OH group of Compound **8** is in the hydrogen bonding distance with the side chain of Arg141, whereas the 6-CH_2OH group of compound **2** is in the hydrogen bonding distance with the side chain of Gln185.

Whereas the 7-CH_2OH group can act as a hydrogen-bond donor as well as a hydrogen-bond acceptor, the 7-CH_2OMe group can only act as a hydrogen-bond acceptor. Because the 7-CH_2OMe or 7-CH_2OH group would interact with Arg141, and should act as a hydrogen-bond acceptor, the 7-CH_2OMe group would be preferred to 7-CH_2OH at this position if the hydrogen bonding interactions are the major factor. In addition, if the 7-CH_2OH or 7-CH_2OMe group interacts with the hydrophobic methylene groups of Arg141, the 7-CH_2OMe group would be preferred to 7-CH_2OH. Comparison of compounds **1** and **8** shows this is indeed the case.

Figure 6 is a plot of the observed and the calculated pIC_{50} values from the three-component CoMFA model (Eq. 1 in Table 3) from the steric and electrostatic fields.

II. CoMFA for binding model 2

Figure 7 shows all the compounds superimposed in the docked conformation of binding mode 2. Binding mode 2 corresponds to the conformation 2b shown in Fig. 2. The best CoMFA model for the 51 substituted maleimides obtained is a three-component model from the steric and electrostatic fields with the following statistics (see Table 3): R^2(cv)=0.296 and SE(cv)=0.915 for the cross-validation, and R^2=0.784 and SE=0.507 for the fitted. F (3,47)=56.784, and Prob. of R^2=0 (3,47)=0.000. The steric contribution of these maleimide analogs toward their inhibitory potency as described by this model is 49%, whereas the electrostatic portion is 51%. The first component explains 51% of the variance in the pIC_{50}, and the

Table 3 CoMFA models for 51 substituted maleimides from the binding modes 1 and 2

				Cross-validation		Fitted		Contribution	
Eq.	Fields	N[a]	L[b]	SE(cv)	R^2(cv)	SE	R^2	Steric	Electrostatic
Binding mode 1									
1	Steric + Electrostatic	51	3	0.854	0.386	0.475	0.811	48%	52%
		51	2	0.857	0.370	0.565	0.726	52%	48%
		51	1	0.901	0.288	0.745	0.513	47%	53%
Binding mode 2									
2	Steric + Electrostatic	51	3	0.915	0.296	0.507	0.784	49%	51%
		51	2	0.956	0.216	0.622	0.668	50%	50%
		51	1	1.026	0.078	0.746	0.512	50%	50%

[a] Number of compounds used in the model

[b] Number of components in the model

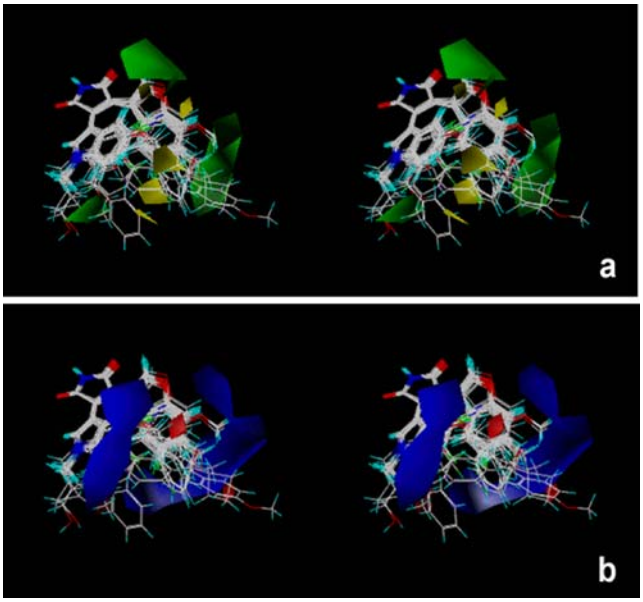

Fig. 4 (**a**) Steric contour of the three-component CoMFA model from the binding mode 1. The regions in green represent sterically favored, whereas the regions in yellow represent disfavored. (**b**) Electrostatic contour of the three-component CoMFA model from the binding mode 1. The regions in blue represent electrostatically favored, whereas the regions in red represent disfavored

second and the third components account for additional 16% and 12% of the variance, respectively. An essentially identical CoMFA model was obtained when the steric and the electrostatic fields were considered separately.

Comparison of two binding modes with CoMFA results

It is interesting to examine the CoMFA results from the two different binding modes of the compounds listed in Table 6:

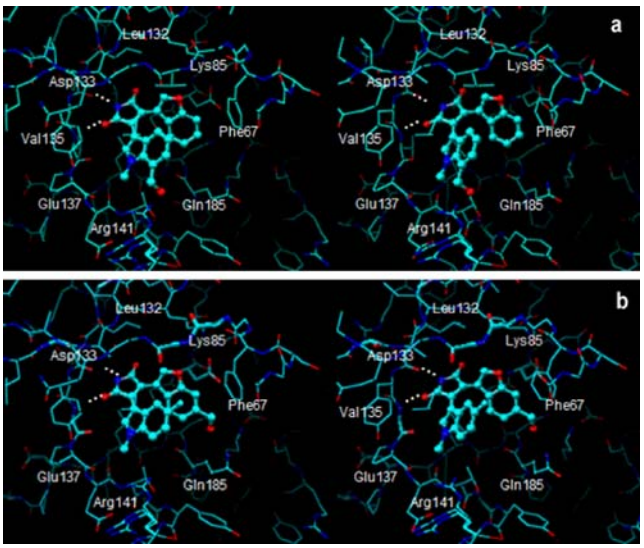

Fig. 5 Docked binding mode of compounds **2** (**a**) or compound **8** (**b**) in the binding site of GSK-3β structure in binding mode 1

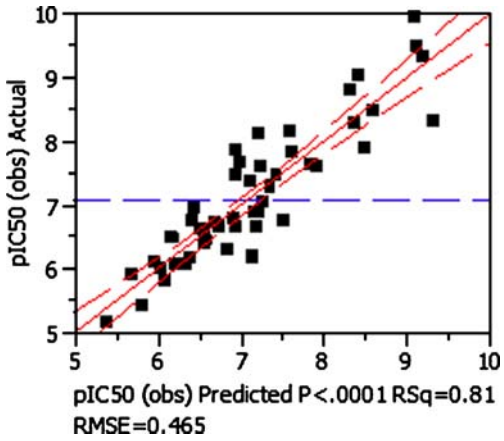

Fig. 6 A plot between the observed and the calculated pIC_{50} values from the three-component CoMFA model of the ligand-binding mode 1

whether the CoMFA results can be used to distinguish the two different binding modes and select the correct binding mode from the wrong one. In general, the two binding modes of the inhibitors alone are not significantly different; the entire molecules are rotated about 180° in the binding pocket as can be seen in Figs. 3, 7, especially for the study of CoMFA. The differences between the two superpositions are due to the different X- and Y-substituents and the environment of the GSK-3β binding site.

The CoMFA results summarized in Table 3 show that the superposition from the binding mode 1 (Eq. 1) accounts for the variation in the pIC_{50} values of the compounds studied more than the superposition from the binding mode 2 (Eq. 2): while Eq. 1 explains 81% of the variance, Eq. 2 explains 78%. Even though the difference between the two results (percent of the variance explained by the two models) is not large, the statistics (SE and R^2 for both the cross-validation and the fitted) indicate that the binding mode 1 is better than binding mode 2. The relatively similar results are due to the similar superposition of the two binding modes. It is interesting, in this case, that the correct and the incorrect binding modes (or superpositions) yielded similar CoMFA results, even though the correct binding

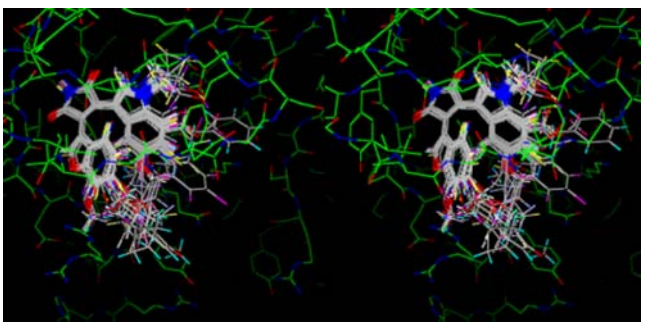

Fig. 7 Superposition of 51 substituted maleimides as GSK-3β inhibitors obtained from docking into the binding site of GSK-3β (1P0E) structure in binding mode 2

mode gave the better results. Usually in CoMFA, the model having R^2(cv)>0.3 is considered significant. Therefore, the CoMFA model for binding mode 2 is at the borderline of statistical significance. Therefore, the results overall indicate that the binding mode 1 would be favored over binding mode 2 for the benzofuran-3-yl-(indol-3-yl)maleimides examined in this study.

Further validation of CoMFA model from binding model 1

In order to further validate the CoMFA model derived from binding mode 1, the inhibitory potency values pIC_{50} were scrambled and used as such to develop a CoMFA model. The resulting CoMFA model was then compared with the CoMFA model developed using the correct pIC_{50} values. Such procedures have been used to prove the robustness of the derived CoMFA model. Five different scrambled pIC_{50} data sets were used in this validation procedure (See Table 4 for further details). The statistics for the CoMFA models developed using the scrambled pIC_{50} values for the 51 substituted maleimides are summarized in Table 4. The results show that none of the scrambled pIC_{50} data sets yielded a statistically significant CoMFA model. The results provide additional support for the CoMFA model derived from binding mode 1 of these compounds.

Comparative molecular similarity index analysis

The two binding modes of the compounds (Figs. 2, 5) in Table 6 used in the CoMFA studies described above were also used to study 3D-QSAR using the CoMSIA approach. The CoMSIA results obtained from binding modes 1 and 2 are summarized in Table 5.

I. CoMSIA for binding model 1

The best CoMSIA model obtained from 51 substituted maleimides in Table 6 is a three-component model from the steric and electrostatic fields with the following statistics (see Table 5): R^2(cv)=0.414 and SE(cv)=0.835 for the cross-validation, and R^2=0.746 and SE=0.550 for the fitted. F (3,47)=45.952, and Prob. of R^2=0 (3,47)=0.000. The steric portion of the influences of maleimide analogs for the inhibitory potency described by this model is 25%, whereas the electrostatic portion is 75%. The first component explains 53% of the variance in the pIC_{50}, and the second and the third component account for additional 14% and 8% of the variance. An essentially identical CoMFA model was obtained when the steric and the electrostatic fields were considered separately. Addition of hydrophobic and/or hydrogen donor or acceptor components did not

Table 4 Validation of CoMFA and CoMSIA models for 51 substituted maleimides from binding mode 1 using scrambling pIC_{50} values

Scramble				Cross-validation		Fitted	
Run[a]	Fields	N	L	SE(cv)	R^2(cv)	SE	R^2
CoMFA (Eq. 1)							
1	Steric + Electrostatic	51	1	1.102	-0.065	0.902	0.287
2	Steric + Electrostatic	51	1	1.057	0.021	0.836	0.387
3	Steric + Electrostatic	51	1	1.042	0.048	0.807	0.430
4	Steric + Electrostatic	51	1	1.098	-0.056	0.828	0.399
5	Steric + Electrostatic	51	1	1.116	-0.090	0.890	0.306
CoMSIA (Eq. 3)							
6	Steric + Electrostatic	51	1	1.194	-0.249	0.928	0.249
7	Steric + Electrostatic	51	1	1.077	-0.016	0.918	0.262
8	Steric + Electrostatic	51	1	1.047	0.040	0.877	0.326
9	Steric + Electrostatic	51	1	1.093	-0.047	0.913	0.270
10	Steric + Electrostatic	51	1	1.130	-0.119	0.923	0.253

[a] The scrambling of the inhibitory potency value (pIC_{50}) values used in this validation were generated as follows: The original pIC_{50} values in the data table were initially sorted by the compounds id (not shown). For scramble run 1, the pIC_{50} values of the entire set of compounds were resorted in ascending order and then the resulting pIC_{50} values in the newly sorted order were assigned to the compounds in the initial order as the scrambled pIC_{50} values. For scramble run 2, the compound id of the entire set of compounds were resorted in ascending order and then the resulting pIC_{50} values in the newly sorted order were assigned to the compounds sorted in the descending order as the scrambled pIC_{50} values. For scramble run 3, the pIC_{50} values of the entire set of compounds were resorted in descending order and then the resulting pIC_{50} values in the newly sorted order were assigned to the compounds in the initial order as the scrambled pIC_{50} values. For scramble run 4, the pIC_{50} values of the entire set of compounds were resorted in ascending order and then the resulting pIC_{50} values in the newly sorted order were assigned to the compounds in the initial order as the scrambled pIC_{50} values. For scramble run 5, the pIC_{50} values of the entire set compounds were resorted in ascending order and then the resulting pIC_{50} values in the newly sorted order were assigned to the compounds sorted in the descending order as the scrambled pIC_{50} values.

Table 5 CoMSIA models for 51 substituted maleimides from binding modes 1 and 2

				Cross-validation		Fitted		Contribution		
Eq.	Fields	N[a]	L[b]	SE(cv)	R^2(cv)	SE	R^2	Ster	Elec	Hydrophob
Binding mode 1										
3	Steric + Electrostatic	51	3	0.835	0.414	0.550	0.746	25%	75%	
		51	2	0.853	0.375	0.621	0.668	25%	75%	
		51	1	0.912	0.271	0.735	0.527	26%	74%	
4	Ster + Elec + Hydrophob	51	3	0.839	0.408	0.557	0.739	18%	52%	30%
		51	2	0.864	0.360	0.622	0.668	17%	51%	32%
		51	1	0.913	0.270	0.755	0.500	16%	46%	38%
Binding mode 2										
5	Steric + Electrostatic	51	2	0.915	0.281	0.638	0.650	22%	78%	
		51	1	0.971	0.174	0.737	0.525	22%	78%	
6	Ster + Elec + Hydrophob	51	2	0.921	0.272	0.603	0.688	14%	54%	31%
		51	1	0.951	0.208	0.758	0.496	13%	47%	40%

[a] Number of compounds used in the model

[b] Number of components in the model

improve the correlation already obtained (However, see further discussion below). It is interesting to note that the calculated pIC_{50} value of compound **1** has the largest deviation (1.258) from the observed pIC_{50} value. Compound **1** was also found to be an outlier in the classical QSAR discussed above. In this aspect, the CoMSIA results are similar to the classical QSAR.

As the validation process for the CoMFA model derived from binding mode 1, the inhibitory potency values pIC_{50} were scrambled and used as such to develop a CoMSIA model. The same five different scrambled pIC_{50} data sets used for the validation of the CoMFA model were used in this validation procedure. The results are also summarized in Table 4. The results show that none of the scrambled pIC_{50} data sets yielded a statistically significant CoMSIA model.

Figure 8 is the coefficient contour map of the three-component CoMSIA model derived from 51 compounds. In this contour map, the sterically favored regions are shown in green. The positive electrostatic contours are shown in blue. The model indicated that there are no sterically disfavored regions and no electrostatically negative regions at this contour level. Table 6 shows the observed and the calculated pIC_{50} values from this three-component CoMSIA model along their observed values. Figure 9 is a plot of the observed and the calculated pIC_{50} values from this model.

II. CoMSIA for binding model 2

The best CoMSIA model obtained from 51 substituted maleimides in Table 6 is a two-component model from the steric and the electrostatic fields with the following statistics (see Table 5): R^2(cv)=0.281 and SE(cv)=0.915 for the cross-validation, and R^2=0.650 and SE=0.638 for the fitted. F (2,48)=44.89, and Prob. of R^2=0 (2,48)= 0.000. The steric portion of the influences of maleimide analogs for the inhibitory potency described by this model is 22%, whereas the electrostatic portion is 78%. The first component explains 53% of the variance in the pIC_{50}, and the second component accounts for additional 13% of the variance. An essentially identical CoMSIA model was obtained when the steric and the electrostatic fields were considered separately. Addition of hydrophobic and/or hydrogen donor or acceptor components did not improve the correlation already obtained.

Comparison of two binding modes with CoMSIA results

In light of the similar CoMFA results from the two different binding modes of the compounds studied, it is interesting to examine the CoMSIA results with respect to the two different binding modes.

The CoMSIA results (Eqs. 3, 4, 5, and 6) summarized in Table 5 show that the superposition from binding mode 1 (Eqs. 3 and 4) accounts for the variation in the pIC_{50} values of the compounds studied more than the superposition from binding mode 2 (Eqs. 5 and 6). These results are consistent with those of the CoMFA discussed above. The differences in statistics between the two CoMSIA results are larger than the corresponding CoMFA results. The statistics of the CoMSIA analyses (SE and R^2 for both the cross-validation and the fitted) also indicate that binding mode 1 explains the variation in pIC_{50} better than binding mode 2. The results further support binding mode 1 as the correct binding modes of the compounds studied. Another inter-

Table 6 Inhibitory potency of 51 GSK-3β inhibitors included in this study

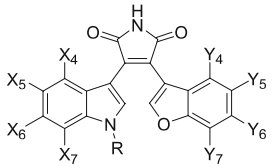

(I)

					pIC50				
				IC50		CoMFA (BM1)		CoMSIA (BM1)	
	X	Y	R	(nM)	Obs	Cal[a]	Dev[a]	Cal[b]	Dev[b]
1	7-CH_2OMe	H	CH_3	0.12	9.921	9.076	0.845	8.663	1.258
2	5-F	6-CH_2OH	CH_3	0.35	9.456	9.114	0.342	8.960	0.496
3	5-Br	6-CH_2OH	CH_3	0.51	9.292	9.196	0.096	8.958	0.334
4	5-F, 6-Cl	6-CH_2OH	CH_3	0.95	9.022	8.409	0.613	8.588	0.434
5	5-Br	H	$(CH_2)_3OH$	1.60	8.796	8.305	0.491	8.221	0.575
6	5-F	6-OH	CH_3	3.50	8.456	8.598	-0.142	7.740	0.716
7	7-CH_2OH	6-CH_2OH	CH_3	5.10	8.292	9.305	-1.013	9.475	-1.183
8	7-CH_2OH	H	CH_3	5.40	8.268	8.371	-0.103	8.442	-0.174
9	5-Br	H	CH_3	7.00	8.155	7.578	0.577	7.602	0.553
10	5-Br	7-OCH_3	CH_3	7.50	8.125	7.182	0.943	7.086	1.039
11	5-CN	6-CH_2OH	CH_3	13.20	7.879	8.495	-0.616	8.188	-0.309
12	6-OH	5-F	CH_3	14.00	7.854	6.916	0.938	6.739	1.115
13	6-OH	H	CH_3	15.00	7.824	7.601	0.223	7.581	0.243
14	5-	5-F	CH_3	22.60	7.646	6.970	0.676	6.733	0.913
15	5-F	6-CH_2OCH_3	CH_3	23.80	7.623	7.848	-0.225	8.190	-0.567
16	5-Br	6-O	CH_3	25.30	7.597	7.913	-0.316	7.647	-0.050
17	5-F	H	CH_3	26.00	7.585	7.209	0.376	7.527	0.058
18	5-I	H	CH_3	34.50	7.462	7.410	0.052	7.658	-0.196
19	H	H	CH_3	35.00	7.456	6.911	0.545	7.038	0.418
20	5-Cl	5-F	CH_3	42.00	7.377	7.099	0.278	7.069	0.308
21	5-Br	6-O	CH_3	48.30	7.316	7.350	-0.034	7.469	-0.153
22	7-OH	H	CH_3	55.00	7.260	7.326	-0.066	7.764	-0.504
23	5-,7-di-Br	7-OCH_3	CH_3	88.70	7.052	7.226	-0.174	7.205	-0.153
24	5-F, 6-Cl	7-OCH_3	CH_3	114.00	6.943	6.424	0.519	6.706	0.237
25	5-OCH_3	H	CH_3	125.00	6.903	7.148	-0.245	6.862	0.041
26	5-CN	5,6-di-F		131.00	6.883	7.196	-0.313	6.825	0.058
27	6-OBn	5-F	CH_3	160.00	6.796	6.880	-0.084	6.026	0.770
28	H	7-OCH_3	CH_3	180.00	6.745	6.381	0.364	6.696	0.049
29	5-I	5-F	CH_3	180.00	6.745	7.505	-0.760	7.290	-0.545
30	5-F, 6-Cl	H	CH_3	184.00	6.735	6.661	0.074	7.244	-0.509
31	5-OBn	H	$(CH_2)_3OH$	220.00	6.658	7.175	-0.517	7.113	-0.455
32	7-OBn	H	CH_3	220.00	6.658	6.918	-0.260	7.071	-0.413
33	5-OCH_3, 6-I	H	CH_3	223.00	6.652	6.703	-0.051	6.948	-0.296
34	5-cyclopropyl	H	CH_3	235.00	6.629	6.495	0.134	6.719	-0.090
35	5-F, 6-I	7-OCH_3	CH_3	247.00	6.607	6.533	0.074	6.736	-0.129
36	benzo[g]	5-,6-di-F	CH_3	314.00	6.503	6.134	0.369	6.354	0.149
37	5-Br	6-O-(*p*-CH_3O)-Bn	CH_3	335.00	6.475	6.160	0.315	5.952	0.523
38	5-F	H	H	360.00	6.444	6.570	-0.126	6.873	-0.429
39	5-OCH_3, 6-Cl	H	CH_3	440.00	6.357	6.536	-0.179	6.513	-0.156
40	H	5-Br	CH_3	550.00	6.260	6.811	-0.551	7.020	-0.760
41	H	5-F	H	670.00	6.174	7.120	-0.946	7.187	-1.013
42	5-OH	H	CH_3	690.00	6.161	7.112	-0.951	7.085	-0.924
43	5,6-Methylenedioxy	5-F	CH_3	708.00	6.150	6.359	-0.209	6.228	-0.078
44	6-CF_3	7-OCH_3	CH_3	831.00	6.080	5.933	0.147	6.486	-0.406
45	5-F, 6-Cl	6-OCH_3	CH_3	866.00	6.062	6.304	-0.242	6.384	-0.322
46	6-OBn	H	CH_3	900.00	6.046	6.195	-0.149	5.968	0.078
47	5-F, 6-Cl-	6-O-	CH_3	1040.00	5.983	6.011	-0.028	6.034	-0.051
48	5-Morpholine-4-yl	H	CH_3	1304.00	5.885	5.670	0.215	5.771	0.114
49	5-OBn	H	H	1650.00	5.783	6.074	-0.291	5.878	-0.095
50	5-F, 6-Cl-	6-O-	CH_3	4092.00	5.388	5.800	-0.412	5.366	0.022
51	5-F, 6-*p*-Cl-Ph	7-OCH_3	CH_3	7000.00	5.155	5.359	-0.204	5.694	-0.539

[a] Calculated using the three-component CoMFA model (Eq. 1) derived from 51 compounds using the binding mode 1

[b] Calculated using the three-component CoMSIA model (Eq. 3) derived from 51 compounds using binding mode 1

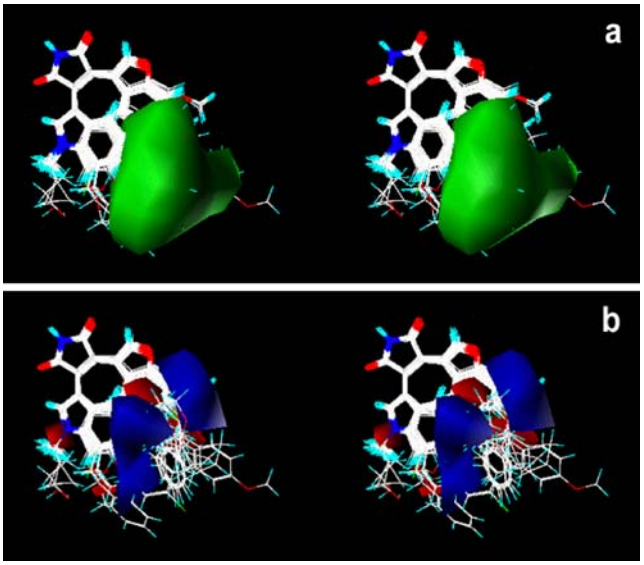

Fig. 8 (**a**) Steric contour map (70% level) of the three-component CoMSIA model. (**b**) Electrostatic contour map (30% level) of the corresponding three-component CoMSIA model in the ligand-binding mode 1

esting aspect of the CoMSIA results is that Eqs. 4 and 6 indicate some possible contributions of hydrophobic contribution of the substituents toward the observed pIC_{50} values as in the classical QSAR discussed above. It was previously studied that the steric contribution of CoMFA may include the hydrophobic contribution [38–43]. The present CoMSIA results indicate separate contributions from the hydrophobic contributions even though the steric contributions may include the hydrophobic contributions of the substituents as in the case of CoMFA.

As in CoMFA, the model having $R^2(cv)>0.3$ may be considered significant in CoMSIA. Therefore, the CoMSIA model for binding mode 2 may not be statistically significant in this standard. Therefore, the results of CoMSIA are consistent with those of CoMFA, and both results indicate that binding mode 1 would be favored over binding mode 2 for the benzofuran-3-yl-(indol-3-yl)maleimides examined in this study.

Comparison of 3D-QSAR results with the current X-ray structures

While this manuscript was in preparation, the preliminary results of ligand-bound X-ray crystal structures of GSK-3β became available. The present 3D-QSAR results are interesting to compare with the preliminary X-ray crystal structures of two GSK-3β inhibitors, namely compound **5** and compound **14**. Compound **5** has Br as X5 and $(CH_2)_3OH$ as R. Compound **14** has 5-cyclopropylethynyl as X5, F as Y5, and CH_3 as R. Even though there are clear differences in the substituent pattern of these two compounds, the initial X-ray crystal structures could not readily discern the relative positions of the indole ring and the benzofuran ring. In fact, the positions of these two rings were thought to be switched and be similar to binding mode 1 in the initial preliminary X-ray results. This initial observation was not consistent with the 3D-QSAR results. In the updated X-ray crystal structures of these two compounds, however, it was determined that the positions of the two rings are consistent with binding mode 1.

The CoMFA results indicate that binding mode 1 is preferred over binding mode 2. The same is true for the CoMSIA results. The CoMSIA results indicate more clearly that binding mode 1 better accounts for the variance in pIC_{50} than does binding mode 2, even though their statistics are inferior to those of CoMFA.

Figure 10 shows a superposition of the docked conformation and the current X-ray crystal structures of compounds **5** and **14**. Figure 10a shows that the docked conformation (shown in purple) and the current X-ray crystal structure (shown in cyan) of compound **5** are essentially identical. Although the superposition of the docked conformation (shown in green) and the X-ray crystal structure (shown in orange) of compound **14** are very similar, Fig. 10b shows that there is some movement in the binding pocket of GSK-3β (See further discussion below about the flexible binding pocket relating to the binding mode of compound **14**).

Unexplained pIC_{50} portions by the 3D-QSAR results

The current CoMFA and CoMSIA models account for the variance of pIC_{50} values about 80% and 75%, (R^2=0.81 for CoMFA and 0.75 for CoMSIA), and the corresponding SE values are 0.48 and 0.55, respectively. Unexplained portion or outliers of QSARs can be very important and interesting, especially when the observed biological activity is higher

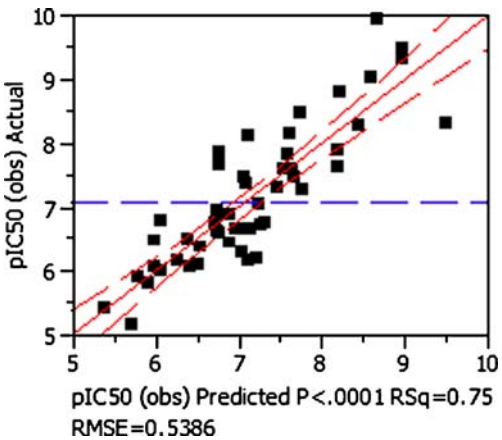

Fig. 9 A plot between the observed and the calculated pIC_{50} values from the three-component CoMSIA model from the steric and electrostatic fields of the ligand-binding mode 1

than that predicted by the QSAR model. Unexplained portions or outliers by the QSAR model may imply several possibilities in addition to experimental errors. They may imply that the QSAR may lack certain descriptors to describe the QSAR of the entire group of compounds studied, or that the mathematical model or approach may not be appropriate. The outliers or unexplained portions may also be due to the inappropriate calculation of the parameter values used, may indicate a different mechanism of action, or may result from a different binding mode or a flexible binding site [44, 45].

One possible source of the unexplained component of the pIC_{50} values in the present case, which is about 20% of the variance in pIC_{50} values, is likely due to the flexible binding pocket as shown in Fig. 1b. Depending on the size of the ligand, the flexible glycine-rich loop of GSK-3β may change its loop conformation as indicated by the different position of Phe67 in the various X-ray crystal structures. (Also see the discussion below for Fig. 10b and compound 14.) Another possible source is the flexible side chain conformation as observed by the different side chain conformations of Arg141 (see the lower left corner of Fig. 1b). The third possibility is the binding mode of the benzofuran ring. The size of the binding pocket where the benzofuran ring binds is large enough to accommodate the unsubstituted benzofuran ring in two different positions. One possibility is the one shown by the binding of the corresponding indole ring in staurosporine (Fig. 1c, 1Q3D) or in the bis-(indole)maleimide pyridinophane (Fig. 1d, 2OW3), and the other is the one seen in the conformation used in the current CoMFA or CoMSIA studies. Interestingly, two different benzofuran binding conformations were observed in the compound **14**-bound GSK-3β X-ray crystal structure which is shown in Fig. 11.

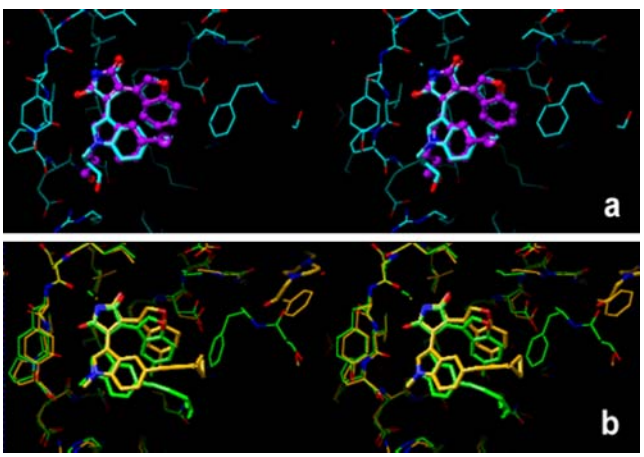

Fig. 10 Superposition of the docked and the preliminary X-ray crystal structures of compounds **5** (**a**) and **14** (**b**). In Fig. 10a, the docked structure of compound **5** is shown in purple, while the X-ray crystal structure of the same compound is shown in cyan. In Fig. 10b, the docked structure of compound **14** is shown in green, while the X-ray crystal structure of the same compound is shown in orange

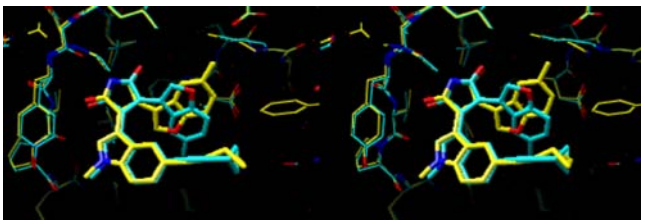

Fig. 11 Two different binding modes of the benzofuran ring of compound **14** observed in the X-ray crystal structure of the ligand-bound GSK-3β

In QSAR, if the difference between the observed and the calculated activity values is greater than twice the standard error of the model, such compounds are normally considered as outliers. Table 6 shows that one compound (compound **7**; X=7-CH_2OH, Y=6-CH_2OH, and R=CH_3) is an outlier of the CoMFA model derived from binding mode 1. The calculated pIC_{50} value of this compound is 9.31, whereas the observed pIC_{50} value is 8.29. The difference is larger than 1.0 in logarithmic unit. Thus, the compound is calculated to be more a potent binder than observed. Possible reasons for the discrepancy between the calculated and the observed inhibitory potencies of this compound could be due to various reasons as described above, as well as to possible experimental error. This discrepancy suggests that this compound might be studied further.

Unlike the CoMFA model, the corresponding CoMSIA model from binding mode 1 yielded five outliers (compounds **1**, **7**, **10**, **12**, and **41**). The larger number of outliers from the CoMSIA model shows that the CoMSIA model does not explain the observed pIC_{50} values as well as the CoMFA model, and is not as good as the corresponding CoMFA model to describe the 3D-QSAR for the set studied. However, it is interesting to see that the CoMSIA model also suggests that compound **7** would be a more potent binder than observed. The difference between the two values is greater than 1.0 in logarithmic unit. These results are consistent with those of CoMFA.

Further utilization of the 3D-QSAR results

The aim of this study was to identify the binding mode of the substituted maleimides (**I**) to the binding site of GSK-3β. Understanding the binding modes of compounds under study is critical in drug discovery research. Utilizing the 3D-QSAR methodologies of both CoMFA and CoMSIA, the possible binding mode of the maleimides of interest was determined in this study. The CoMFA model was further validated statistically using the scrambled pIC_{50} values. The suggested binding modes of these compounds were further supported by the two preliminary X-ray crystal structures of inhibitor-bound GSK-3β.

Even though the major aim of our study was accomplished, it was interesting to test the CoMFA model

developed from binding mode 1 for its predictability. Two compounds were synthesized and their pIC_{50} values were estimated using the final CoMFA and CoMSIA models while they were being tested for their biological activity. One compound (**52**) is X5=Cl, X6=OMe, R=CH_3, and the other compound (**53**) is X7=CH_2OMe, Y6=CH_2OH, R=CH_3. The calculated pIC_{50} values from the CoMFA model are 6.13 for compound **52** and 7.67 for compound **53**. The calculated pIC_{50} values from the CoMSIA model are 5.95 for compound **52** and 5.77 for compound **53**. The experimentally determined pIC_{50} values are 7.09 (81.4 nM) and 9.14 (0.73 nM) for compound **52** and **53**, respectively. The experimentally determined pIC_{50} values are higher than the calculated values for both compounds from both CoMFA and CoMSIA methods. Although compound **53** is not the most potent inhibitor in this series, it is still significantly potent. It provides an example of utilizing the binding mode and 3D-QSAR of these GSK-3β inhibitors in our drug discovery research. The results of CoMFA fit better than the results of CoMSIA.

Although we were delighted to see the higher inhibitory potencies of the newly synthesized compounds, it was also puzzling to see the poor predictabilities of both 3D-QSAR models, at least for these two compounds. For compound **52** (5-Cl, 6-OCH_3), one can compare the results with those of compound **39** (5-OCH_3, 6-Cl). The observed pIC_{50} of compound **39** is 6.36, whereas the calculated values are 6.54 and 6.51 from CoMFA and CoMSIA, respectively. One can see that while both 3D-QSAR models predicted well the pIC_{50} value of Compound **39**, those models did not predict well the pIC_{50} value of compound **52**. The results indicate that the current models do not describe the effects of these structural changes on the inhibitory potencies. However, inclusion of these two compounds in the further development of the CoMFA and CoMSIA models could improve the predictabilities of both models for future compounds containing such structural modifications. If a 3D-QSAR model does not contain certain structural information, it is not surprising to find that the model is generally unable to predict the activity of a compound embodying such structural modifications [30].

Summary and conclusions

The binding modes of GSK-3β inhibitors have been studied with molecular modeling and docking methods along with 3D-QSAR approaches. The approaches of CoMFA and CoMSIA were used for 3D-QSAR with 51 substituted benzofuran-3-yl-(indol-3-yl)maleimides as GSK-3β inhibitors.

Two binding modes of our inhibitors to the binding pocket of GSK-3β were investigated. Binding mode 1 yielded better CoMFA and CoMSIA correlations. The binding mode determined by the results of this study is consistent with the preliminary results of an X-ray crystal structure analysis of inhibitor-bound GSK-3β. This study shows that the 3D-QSAR methodologies are useful in identifying the correct binding modes of the substituted benzofuran-3-yl-(indol-3-yl)maleimides to GSK-3β. These models will be updated with additional compounds and used in our continued work to estimate the inhibitory potency of other novel GSK-3β inhibitors of this structural class.

Several possible sources of the unexplained component of the pIC_{50} values by the 3D-QSAR models are discussed.

The present study provides the first example of identifying the correct binding mode of GSK-3β inhibitors using the molecular modeling, docking, and 3D-QSAR approaches.

Experimental section

The publicly available protein structures used in this study and listed in Table 1 were obtained from the RSCS protein data bank [34].

Two binding modes of the 51 compounds in the GSK-3β binding site were obtained by docking each compound into the binding site (see the discussions in the text) starting from the initial 2a and 2b conformations in Table 2.

The ligands were manually docked into the binding site of GSK-3β (1R0E). The initial binding position of the ligands was set by superimposing the pyrrolidin-2-one ring of the inhibitors over the corresponding ring of the ligand in the ligand-bound X-ray crystal structure of GSK-3β, 1R0E.

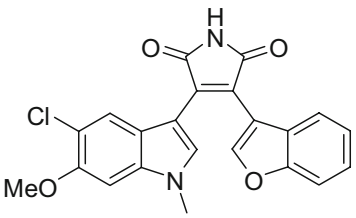

(**52**)

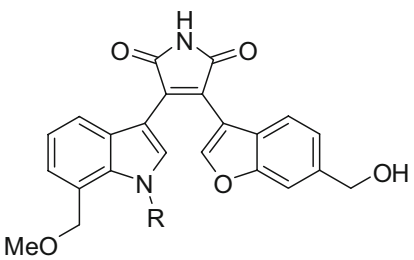

(**53**)

Initial docking conformations of the substituted indole ring and the substituted benzofuran ring of the inhibitors were set to be similar to the two conformations (2a and 2b) shown in Fig. 2. The orientation of each side chain of the molecules were set in such a way that the substituents would exhibit minimal steric clashes with any amino acid residues of the protein, but would be able to engage in possible hydrogen bonding interactions with nearby amino acid residues.

The geometry optimizations of the ligand-bound GSK-3β complexes were then performed using the molecular modeling software Sybyl version 7.3 of Tripos. The optimization of the protein-ligand complex was done by the Powell method without any initial optimization using the MMFF94 force field, the Gasteiger-Marsili charges, constant dielectric function, NB cut-off of 8.0, and dielectric constant of 1.0. The default settings were used for others with termination when the gradient reaches 0.05 kcal mol^{-1}. The maximum iteration for the geometry optimizations was set to be 1000.

The 3D-QSAR models were developed using the techniques of CoMFA and CoMSIA available in the Sybyl software package. The superpositions of the inhibitors used for each CoMFA and CoMSIA models were those of the docked positions and conformations obtained as described above. The CoMFA and CoMSIA modules of the molecular modeling software Sybyl version 7.3 of Tripos were used for these 3D-QSAR analyses. Default settings for all parameters were used using CH_3^+ as the probe, a 2-angstrom lattice box, and the Gasteiger-Marsili charges. Leave-one-out method was used for the cross-validation step. The PLS analysis was done using the SAMPLS method available through Sybyl. The selections of the final CoMFA and CoMSIA models were based on the results of the cross-validation, and are summarized in Table 3 (CoMFA) and Table 5 (CoMSIA). Further validation of the CoMFA and CoMSIA models from binding mode 1 using scrambling pIC_{50} values are summarized in Table 4.

All the figures were generated using the UCSF chimera molecular modeling program production version 1 [46].

Acknowledgments Ki Kim thanks Dr. Pavel Petukhov for the use of molecular modeling software. Andrew Mesecar is supported by grants from the National Cancer Institute of the National Institutes of Health (CA92744 and CA48112). This work was supported in part by NIH grant (1R01 MH072940-01, Grantee Alan P. Kozikowski)

References

1. Martinez A (2008) Preclinical efficacy on GSK-3 inhibitors: Towards a future generation of powerful drugs. Med Res Rev 5:773–796
2. Jope RS, Yuskaitis CJ, Beurel E (2007) Glycogen synthase kinase-3 (GSK3): Inflammation diseases and therapeutics. Neurochem Res 32:577–595
3. Bhat R, Haeberlein SLB, Avila J (2004) Glycogen synthase kinase 3: a drug target for CNS therapies. J Neurochem 89:1313–1317
4. Martinez A, Castro A, Alonso M (2002) Glycogen synthase kinase 3 (GSK-3) inhibitors as new promising drugs for diabetes, neurodegeneration, cancer, and inflammation. Med Res Rev 22:373–384
5. Martinez A, Alonso M, Castro A, Pérez C, Moreno FJ (2002) First non-atp competitive glycogen synthase kinase 3 (GSK-3) inhibitors: thiadiazolidinones (TDZD) as potential drugs for the treatment of alzheimer′s disease. J Med Chem 45:1292–1299
6. Meijer L, Skaltsounis AL, Magiatis P, Polychronopoulos P, Knockaert M, Leost M, Ryan XP, Vonica CA, Brivanlou A, Dajani R, Crovace C, Tarricone C, Musacchio A, Roe SM, Pearl L, Greengard P (2003) GSK-3-selective inhibitors derived from Tyrian purple indirubins. Chem Biol 10:1255–1266
7. Kuo G-H, Prouty C, DeAngelis A, Shen LQ, O′Neill DJ, Shah C, Connolly PJ, Murray WV, Conway BR, Cheung P, Westover L, Xu JZ, Look RA, Demarest KT, Emanuel S, Middleton SA, Jolliffe L, Beavers MP, Chen X (2003) Synthesis and discovery of macrocyclic polyoxygenated bis-7-azaindolylmaleimides as a novel series of potent and highly selective glycogen synthase kinase-3â inhibitors. J Med Chem 46:4021–4031
8. Witherington J, Bordas V, Gaiba A, Garton NS, Naylor A, Rawlings AD, Slingsby BP, Smith DG, Takle AK, Ward RW (2003) 6-Aryl-pyrazolo[34-b]pyridines: potent inhibitors of glycogen synthase kinase-3 (GSK-3). Bioorg Med Chem Lett 13:3055–3057
9. Witherington J, Bordas V, Gaiba A, Naylor A, Rawlings AD, Slingsby BP, Smith DG, Takle AK, Ward RW (2003) 6-Heteroaryl-pyrazolo[34-b]pyridines: potent and selective inhibitors of glycogen synthase kinase-3 (GSK-3). Bioorg Med Chem Lett 13:3059–3062
10. Bregman H, Williams D, Atilla GE, Carroll PJ, Meggers E (2004) An organometallic inhibitor for glycogen synthase kinase 3. J Am Chem Soc 126:13594–13595
11. Engler TA, Henry JR, Malhotra S, Cunningham B, Furness K, Brozinick J, Burkholder TP, Clay MP, Clayton J, Diefenbacher C, Hawkins E, Iversen PW, Li Y, Lindstrom TD, Marquart AL, McLean J, Mendel D, Misener E, Briere D, O'Toole JC, Porter WJ, Queener S, Reel JK, Owens RA, Brier RA, Eessalu TE, Wagner JR, Campbell RM, Vaughn R (2004) Substituted 3-imidazo[12-a]pyridin-3-yl-4-(1234-tetrahydro-[14]diazepino-[671-hi]indol-7-yl) pyrrole-25-diones as highly selective and potent inhibitors of glycogen synthase kinase-3. J Med Chem 47:3934–3937
12. Kunick C, Laurenroth K, Wieking K, Xie X, Schultz C, Gussio R, Zaharevitz D, Leost M, Meijer L, Weber A, Jorgensen FS, Lemcke T (2004) Evaluation and comparison of 3D-QSAR CoMSIA models for CDK1, CDK5, and GSK-3 inhibition by paullones. J Med Chem 47:22–36
13. Peat AJ, Garrido D, Boucheron JA, Schweiker SL, Dickerson SH, Wilson JR, Wang TY, Thomson SA (2004) Novel GSK-3 inhibitors with improved cellular activity. Bioorg Med Chem Lett 14:2127–2130
14. Meijer L, Flajolet M, Greengard P (2004) Pharmacological inhibitors of glycogen synthase kinase 3. Trends Pharmacol Sci 9:471–480
15. Zhang HC, Ye H, Conway BR, Derian CK, Addo MF, Kuo GH, Hecker LR, Croll DR, Li J, Westover L, Xu JZ, Look R, Demarest KT, Andrade-Gordon P, Damiano BP, Maryanoff BE (2004) 3-(7-Azaindolyl)-4-arylmaleimides as potent selective inhibitors of glycogen synthase kinase-3. Bioorg Med Chem Lett 14:3245–3250

16. Polychronopoulos P, Magiatis P, Skaltsounis AL, Myrianthopoulos V, Mikros E, Tarricone A, Musacchio A, Roe SM, Pearl L, Leost M, Greengard P, Meijer L (2004) Structural basis for the synthesis of indirubins as potent and selective inhibitors of glycogen synthase kinase-3 and cyclin-dependent kinases. J Med Chem 47:935–946
17. Martinez A, Alonso M, Castro A, Dorronsoro I, Gelpi JL, Luque FJ, Perez C, Moreno FJ (2005) SAR and 3D-QSAR studies on thiadiazolidinone derivatives: exploration of structural requirements for glycogen synthase kinase 3 inhibitors. J Med Chem 48:7103–7112
18. Zeng M, Jiang Y, Zhang B, Zheng K, Zhang N, Yu Q (2005) 3D QSAR studies on GSK-3 inhibition by aloisines. Bioorg Med Chem Lett 15:395–399
19. Kozikowski AP, Gaisina IN, Petukhov PA, Sridhar J, King LT, Blond SY, Duka T, Rusnak M, Sidhu A (2006) Highly potent and specific GSK-3b inhibitors that block tau phosphorylation and decrease a-synuclein protein expression in a cellular model of parkinson's disease. Chem Med Chem 1:256–266
20. Dessalew N, Bharatam PV (2007) 3D-QSAR and molecular docking study on bisarylmaleimide series as glycogen synthase kinase 3 cyclin dependent kinase 2 and cyclin dependent kinase 4 inhibitors: An insight into the criteria for selectivity. Eur J Med Chem 42:1014–1027
21. Dessalew N, Patel DS, Bharatam PV (2007) 3D-QSAR and molecular docking studies on pyrazolopyrimidine derivatives as glycogen synthase kinase-3beta inhibitors. J Mol Graph Model 25:885–895
22. Hamann M, Alonso D, Martin-Aparicio E, Fuertes A, Perez-Puerto MJ, Castro A, Morales S, Navarro ML, del Monte-Millan M, Medina M, Pennaka H, Balaiah A, Peng J, Cook J, Wahyuono S, Martinez A (2007) Glycogen synthase kinase-3 (GSK-3) inhibitory activity and structure–activity relationship (SAR) studies of the manzamine alkaloids potential for alzheimer's disease. J Nat Prod 70:1397–1405
23. Shin D, Lee SC, Heo YS, Cho YS, Kim YE, Hyun YL, Cho JM, Lee YS, Ro S (2007) Design and synthesis of 7-hydroxy-1H-benzoimidazole derivatives as novel inhibitors of glycogen synthase kinase-3beta. Bioorg Med Chem Lett 17:5686–5689
24. Kozikowski AP, Gaisina IN, Yuan H, Petukhov PA, Blond SY, Fedolak A, Caldarone B, McGonigle P (2007) Structure-based design leads to the identification of lithium mimetics that block mania-like effects in rodents. possible new GSK-3β therapies for bipolar disorders. J Am Chem Soc 129:8328–8332
25. Stukenbrock H, Mussmann R, Geese M, Ferandin Y, Lozach O, Lemcke T, Kegel S, Lomow A, Burk U, Dohrmann C, Meijer L, Austen M, Kunick C (2008) 9-Cyano-1-azapaullone (Cazpaullone. a Glycogen Synthase Kinase-3 (GSK-3) inhibitor activating pancreatic β Cell protection and replication. J Med Chem 51:2196–2207
26. Voigt B, Krug M, Schachtele C, Totzke F, Hilgeroth A (2008) Probing Novel 1-Aza-9-oxafluorenes as selective GSK-3b inhibitors. Chem Med Chem 3:120–126
27. Taha MO, Bustanji Y, Al-Ghussein MAS, Mohammad M, Zalloum H, Al-Masri IM, Atallah N (2008) Pharmacophore modeling quantitative structure-activity relationship analysis, and in silico screening reveal potent glycogen synthase kinase-3 inhibitory activities for cimetidine, hydroxychloroquine, and gemifloxacin. J Med Chem 51:2062–2077
28. Gaisina IN, Gallier F, Kim KH, Ougolkov AV, Guo S, Holzle D, Luchini DN, Kurome T, Blond SY, Billadeau D, Kozikowski AP. Identification of Potent and Selective GSK-3β Inhibitors that Suppress Proliferation and Survival of Pancreatic Cancer Cells. J Med Chem 52:1853–1863
29. Kim KH (1995) Comparative molecular field analysis. In: Dean PM (ed) Molecular similarity in drug design. Chapman & Hall, London, pp 291–331
30. Kim KH, Greco G, Novellino E (1998) A critical review of recent CoMFA applications. Perspect Drug Discovery Des 12–14:233–255
31. Martin YC, Kim KH, Lin CT (1996) Comparative Molecular Field Analysis: CoMFA, vol 1. JAI Press, pp 1-52
32. Klebe G (1998) Comparative molecular similarity indices analysis: CoMSIA. In: Kubinyi HFG, Martin YC (eds) Three-dimensional quantitative structure activity relationships, 3d qsar in drug design, recent advances. Vol 3. Springer, Netherlands, pp 87–104
33. Bertrand JA, Thieffine S, Vulpetti A, Cristiani C, Valsasina B, Knapp S, Kalisz HM, Flocco M (2003) Structural characterization of the GSK-3β active site using selective and non-selective ATP-mimetic inhibitors. J Mol Biol 333:393–407
34. Berman HM, Westbrook J, Feng Z, Weissig H, Shindyalov IN, Bourne PE (2000) The protein data bank. Nucleic Acids Res 28:235–242
35. Hubbard SR (2000) Protein tyrosine kinase structure and function. Annu Rev Biochem 69:373–398
36. Huse M (2002) The conformational plasticity of protein kinases. Cell 109:275–282
37. Johnson LN (1996) Active and inactive protein kinases: structural basis for regulation. Cell 85:149–158
38. Kim KH (1991) A novel method of describing hydrophobic effects directly from 3D Structures in 3D-quantitative structure-activity relationships study. Med Chem Res 1:259–264
39. Kim KH (1992) Description of nonlinear dependence directly from 3D structures in 3D-quantitative structure-activity relationships. Med Chem Res 2:22–27
40. Kim KH (1992) Quantitative structure-activity relationships: nonlinear dependence described directly from 3D structures using comparative molecular field analysis (CoMFA). Quant Struct-Act Relat 11:309–317
41. Kim KH (1993) Nonlinear dependence in GRID-comparative molecular field analysis (CoMFA). J Comput Aid Mol Design 7:71–82
42. Kim KH (1993) Quantitative structure-activity relationships: describing hydrophobic interactions directly from 3D structures using a comparative molecular field analysis (CoMFA) approach. Quant Struct-Act Relat 12:232–238
43. Kim KH (1995) Calculation of hydrophobic parameters directly from three-dimensional structures using comparative molecular field analysis (CoMFA). J Comput Aid Mol Design 9:308–318
44. Kim KH (2007) Outliers in SAR and QSAR: 2 is flexible binding site a possible source of outliers? J Comput Aid Mol Design 21:421–435
45. Kim KH (2007) Outliers in SAR and QSAR: is unusual binding mode a possible source of outliers? J Comput Aid Mol Design 21:63–86
46. Pettersen EF, Goddard TD, Huang CC, Couch GS, Greenblatt DM, Meng EC, Ferrin TE (2004) UCSF Chimera - a visualization system for exploratory research and analysis. J Comput Chem 25:1605–1612
47. Allard J, Nikolcheva T, Gong L, Wang J, Dunten P, Avnur Z, Waters R, Sun Q, Skinner B. From genetics to therapeutics: the Wnt pathway and osteoporosis, *to be published*
48. Zhang HC, Bonaga LV, Ye H, Derian CK, Damiano BP, Maryanoff BE (2007) Novel bis(indolyl) maleimide pyridinophanes that are potent selective inhibitors of glycogen synthase kinase-3. Bioorg Med Chem Lett 17:2863–2868
49. Bax B, Carter PS, Lewis C, Guy AR, Bridges A, Tanner R, Pettman G, Mannix C, Culbert AA, Brown MJ, Smith DG, Reith AD (2001) The structure of phosphorylated GSK-3beta complexed with a peptide FRATtide that inhibits beta-catenin phosphorylation. Structure 9:1143–1152
50. Dajani R, Fraser E, Roe SM, Yeo M, Good VM, Thompson V, Dale TC, Pearl LH (2003) Structural basis for recruitment of

glycogen synthase kinase 3beta to the axin-APC scaffold complex. EMBO J 22:494–501
51. Bertrand JA, Thieffine S, Vulpetti A, Cristiani C, Valsasina B, Knapp S, Kalisz HM, Flocco M (2003) Structural characterization of the GSK-3beta active site using selective and non-selective ATP-mimetic inhibitors. J Mol Biol 333:393–407
52. Dajani R, Fraser E, Roe SM, Young N, Good V, Dale TC, Pearl LH (2001) Crystal structure of glycogen synthase kinase 3 beta: structural basis for phosphate-primed substrate specificity and autoinhibition. Cell 105:721–732
53. ter Haar E, Coll JT, Austen DA, Hsiao HM, Swenson L, Jain J (2001) Structure of GSK3beta reveals a primed phosphorylation mechanism. Nat Struct Biol 8:593–596
54. Aoki M, Yokota T, Sugiura I, Sasaki C, Hasegawa T, Okumura C, Ishiguro K, Kohno T, Sugio S, Matsuzaki T (2004) Structural insight into nucleotide recognition in tau-protein kinase I/glycogen synthase kinase 3 beta. Acta Crystallogr Sect D 60:439–446
55. Bhat R, Xue Y, Berg S, Hellberg S, Ormo M, Nilsson Y, Radesater AC, Jerning E, Markgren PO, Borgegard T, Nylof M, Gimenez-Cassina A, Hernandez F, Lucas JJ, Diaz-Nido J, Avila J (2003) Structural insights and biological effects of glycogen synthase kinase 3-specific inhibitor AR-A014418. J Biol Chem 278:45937–45945
56. Kim HJ, Choo H, Cho YS, No KT, Pae AN (2008) Novel GSK-3b inhibitors from sequential virtual screening. Bioorg Med Chem 16:636–643
57. GSK-3β *in vitro* kinase assay was done as described previously: The *in vitro* kinase assay was performed in a 40 μL reaction volume containing 250 ng GSK-3β Calbiochem, 10 μM pGS peptide (RRRPASVPPSPSLRHSS(P)HQRR), 10 μM ATP, plus 1 μCi γ32P ATP and increasing concentrations of the inhibitors in kinase buffer (20 mM MOPS pH 7.2, 15 mM $MgCl_2$, 2 mM EGTA, 25 mM β-glycerol phosphate, 1 mM Na_3VO_4, 1 mM DTT). The inhibitors were allowed to bind GSK-3β for 10 min prior to the addition of peptide. The reaction was started by the addition of the ATP solution and was carried out at 30 °C for 30 min after which 25 μL of the reaction mixture was spotted on P81 Whatman filters, dried, washed twice with 0.75% H_3PO_4, and rinsed with acetone. The dried filters were placed in scintillation vials containing 2 ml of Scinti-safe Econo 2 solution and read in a Beckman Coulter LS 600IC scintillation counter. IC_{50} determination as below: The data were plotted as average percent activity versus the log of the concentration of inhibitor. The IC_{50} was determined according to NIH guidelines and the 4-parameter logistic plot (4PL), which calculates the relative IC_{50} based on the maximum (top) and minimum (bottom) percent activity as well as the Hill slope. In some cases the 4PL did not give an accurate fitting of the data (error fit above 40%) and thus a 3-parameter logistic fit top (3PLFT) or 3-parameter logistic fit bottom (3PLFB) were used to obtain the IC_{50} using the equation y = Bottom + (Top-Bottom)/(1 + 10^((LogIC$_{50}$-x)*HillSlope)) from Graphpad Prism 5. This program displays the LogIC_{50} as well as the IC_{50} and gives the standard error of the LogIC_{50}, this was converted back to the % fitting error of the IC_{50} by using the equation %FE (IC_{50}) = FE(LogIC_{50})*Ln(10)*100.